Korean J. Electron Microscopy Special Issue 1, 25~33(2006)

A New Trend of In-situ Electron Microscopy with Ion and Electron Beam Nano-Fabrication

Kazuo Furuya* and Miyoko Tanaka
National Institute for Materials Science (NIMS), 3-13 Sakura, Tsukuba, Ibaraki, 305-0003, Japan
(Received May 7, 2005; Accepted March 24, 2006)

ABSTRACT

Nanofabrication with finely focused ion and electron beams is reviewed, and position and size controlled fabrication of nano-metals and -semiconductors is demonstrated. A focused ion beam (FIB) interface attached to a column of 200 keV transmission electron microscope (TEM) was developed. Parallel lines and dots arrays were patterned on GaAs, Si and SiO_2 substrates with a 25 keV Ga^+-FIB of 200 nm beam diameter at room temperature. FIB nanofabrication to semiconductor specimens caused amorphization and Ga injection. For the electron beam induced chemical vapor deposition (EBI-CVD), we have discovered that nano-metal dots are formed depending upon the beam diameter and the exposure time when decomposable gases such as $W(CO)_6$ were introduced at the beam irradiated areas. The diameter of the dots was reduced to less than 2.0 nm with the UHV-FE-TEM, while those were limited to about 15 nm in diameter with the FE-SEM. Self-standing 3D nanostructures were also successfully fabricated.

Key words : Beam induced CVD, Decomposition, Electron beam, Drilling, Focused ion beam, Nanodots, Nanoparticles

INTRODUCTION

The combination of ion and electron beams with transmission electron microscopes (TEMs) has resulted in the highest quality of nano-fabrication of materials (Matsui & Ichihashi, 1988; Assayag et al., 1993; Aristov et al., 1995; Tanaka et al., 1996; Silvis-Cividjian et al., 2003). In-situ high-resolution electron microscopy (HRTEM) enables to visualize the atomic structure of materials in real space. Typically, focused ion beam (FIB) systems coupled with scanning electron microscopes (SEMs) have an advantage over conventional beam lithography techniques in point of views of highly precision positioning and chemical mapping by energy dispersive X-ray spectroscopy (EDS). Furthermore, ion and electron beams can be used for "active operation of materials in atomic scale" when a TEM is substituted for a SEM, because of its short wavelength which can result in much smaller resolution than several 10 nm (Folch et al., 1995; Koops et al., 1996; Utke et al., 2000). The probe size of electron beams can be reduced to subnanometers in field emission (scanning) transmission electron microscopes (FE-TEMs and FE-STEMs). This would lead to the reduction in size of the fabricated structures in the range of 1.0 nm.

In this paper, we firstly describe a focused ion beam (FIB) interface attached to a column of 200 keV TEM which was developed for in-situ nanofabrication of semiconductors (Furuya & Saito, 1996a, b; Tanaka et al., 1997a, b). One of the conventional methods to investigate the structural changes in FIB irradiated specimens is cross-sectional TEM (XTEM) in which the samples are thinned ex-situ from the direction perpendicular to FIB nanofabricated surface. This method has a problem of fixing the position of interest in the specimens in submicron scale. Our system (FIB/TEM) (Furuya & Saito, 1996a, b) enables the FIB microlithography inside

* Correspondence should be addressed to Dr. Kazuo Furuya, National Institute for Materials Science (NIMS), 3-13 Sakura, Tsukuba, Ibaraki, 305-0003, Japan. Ph.: 81-29-863-5367, FAX: 81-29-863-5571, E-mail: FURUYA.Kazuo1@nims.go.jp

the column of the TEM, and simultaneous observation allows to analyze the structural evolution directly without the artifacts often induced by standard XTEM specimen preparation process.

Secondly, the electron beam induced chemical vapor deposition (EBI-CVD) with a FE-SEM, FE-STEM and ultrahigh vacuum FE-TEM (UHV-FE-TEM) by using metal-organic gas introduction systems is reviewed in detail. EBI-CVD has mainly been performed in SEMs (Folch et al., 1995; Koops et al., 1996; Utke et al., 2000). However, the smallest structures fabricated in SEMs have a typical width of 15~20 nm, no mater how small the primary electron beam is (Kohlmann-von Platen et al., 1993). This is usually attributed to the fact that the distribution of secondary electron, rather than primary electron, determines the size of the deposits. The profile of the secondary electrons has some spread, especially for the energy range of the SEMs. Even for the primary electron of zero-diameter, the profile of the secondary electron spreads more than 15 nm (Silvis-Cividjian et al., 2002). Hence it has been believed that the resolution limit of EBI-CVD is at most 15 nm. However, we have tried to minimize the secondary electron effect by using FE-STEMs (Mitsuishi et al., 2003; Shimojo et al., 2004; Tanaka et al., 2004, 2005). Mitsuishi et. al. successfully fabricated nano-dots of 3.5 nm in diameter using a 200 keV FE-STEM (Mitsuishi et al., 2003). They found that the dot size does not have dependence on the substrate thickness; it is rather the deposition period and speed which strongly affect the dot size. Here, we emphasize the importance of small sized probe and UHV condition on EBI-CVD of various nanostructures.

FIB INTERFACE WITH 200 keV TEM (FIB/TEM)

1. FIB experimentals

In-situ observation of FIB microlithography in TEMs requires submicron ion beams on the sample position in the center of the pole-piece of the objective lens. The TEM used in the present study is JEM-200CX with a side entry stage and scanning TEM (STEM) capability. The FIB system generates a relatively low energy (5~25 keV) Ga beam with a liquid metal ion source (LMIS). Figure 1 illustrates a schematic drawing of the 200 keV TEM column. Ion beams are introduced along the upper

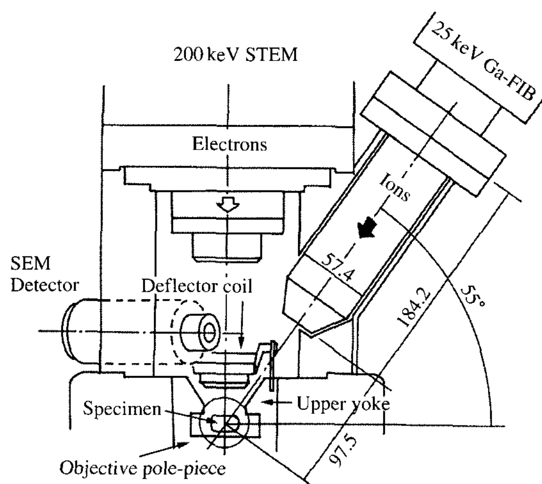

Fig. 1. Schematic diagram of the 200 keV transmission electron microscope (TEM) interfaced with a 25 keV Ga^{+}-FIB system and a SE detector.

yoke of the objective lens of the TEM with an incident beam angle of 35° with respect to the electron beam. The working distance of the FIB is 97.5 mm. The FIB is controlled by both analog scan signals from the STEM unit and digital signals from a PC-based computer.

Samples used in the present study are prepared from Si (001), GaAs (001) and SiO_2 (101) substrates, polished properly to thin films for TEM observation. After the insertion of the samples into the TEM column, the FIB was exactly focused on the area observed with the TEM by adjusting the deflector control of the ion beam system. The FIB energy is 25 keV with a beam diameter of about 200 nm and a beam current of about 70~80 pA. The FIB lithography is carried out at room temperature with a sample tilt of 35 degrees to set ion beams normal to the surface. A set of lines and arrays of dots were patterned by blanking and drawing of ion beams. The scanning speed of FIB was 1.5~2.0 μm/s, corresponding to a Ga ion dose of $1.1 \sim 1.6 \times 10^{17}$ ions/cm^2. TEM images are recorded via video tape during the FIB operation, and TEM photographs are taken after the operation.

2. FIB results and discussion

Figure 2 shows TEM photographs of nanofabricated Si (100) specimen by the FIB in the line scanning mod-

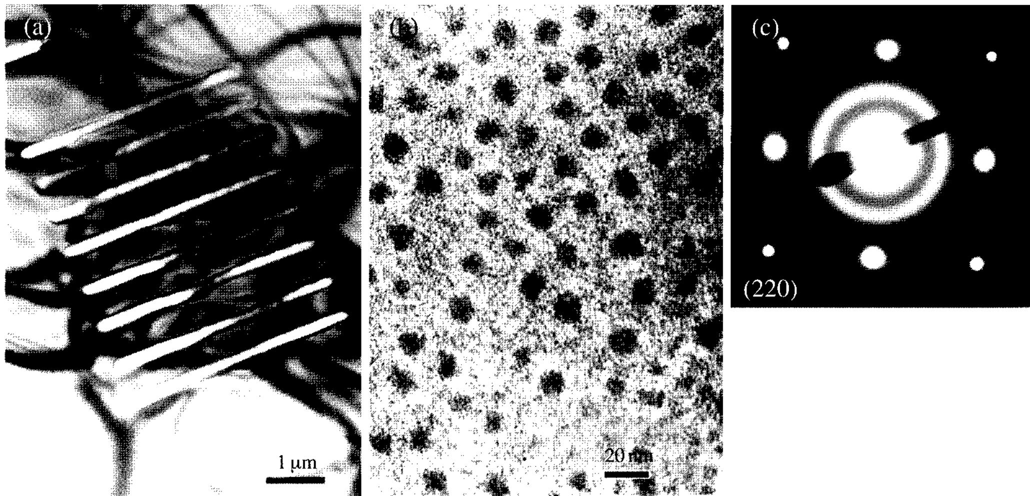

Fig. 2. TEM micrographs of the FIB-micromilled Si (001) sample. (a) 8 parallel lines at intervals of 500 nm, (b), (c) enlarged images of the FIB-microfabricated area showing precipitates about 10 nm in size and (d) its SAD pattern showing polycrystallization.

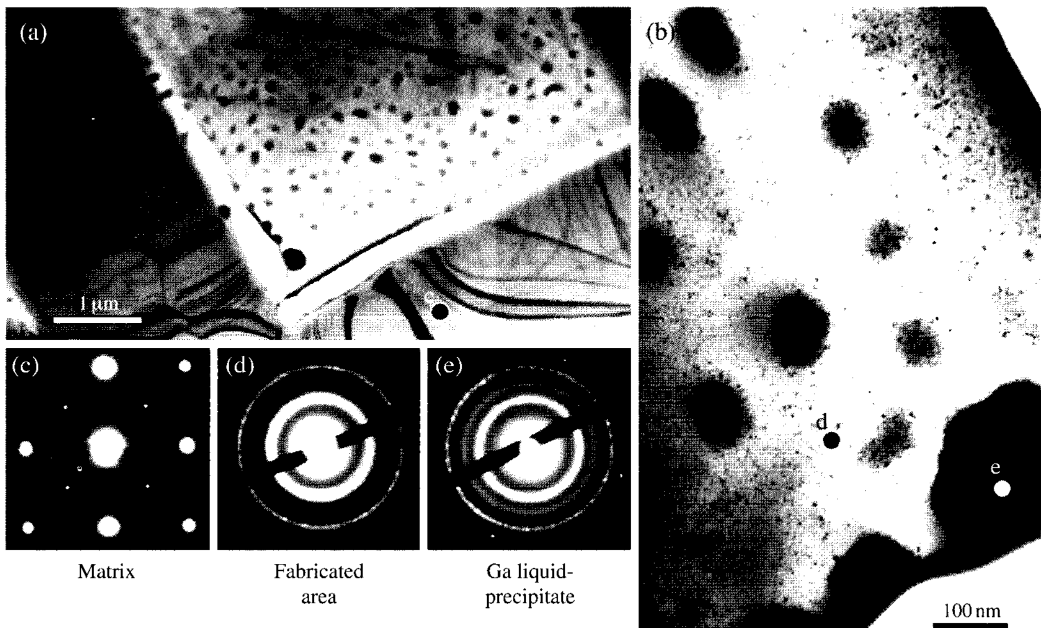

Fig. 3. A set of TEM photographs of GaAs (100) microfabricated by Ga-FIB. (a) bright field image at low magnification, (b) liquid or amorphous precipitates, (c)-(e) elected area diffraction patterns corresponding to points A-C in the figure.

es. 8 parallel lines were fabricated by the FIB at intervals of 500 nm with the width of about 200 nm, which is the same as the beam spot size. The uniform fabrication inside the grooves and the discontinuity of the

bend contours at the boundary of the fabrication are clearly seen. The magnified picture in figure 2-b) indicates many small dark dots about 10 nm in size, which spread in the fabricated area and hollow rings in the SAD pattern in figure 2-c) shows the tendency toward the amorphization. It is reported that the low energy (8 keV) of Ga-FIB applied to Si (100) specimen resulted in the implantation of Ga and the formation of metastable Ga precipitates (Furuya & Ishikawa, 1992). Taking account of the melting point of Ga and of little solid solubility of Ga in Si (White et al., 1980), the structure in figure 2-b) can be the results of the implantation and precipitation of Ga even though the sputtering by Ga ions is dominant on the surface of specimens.

Figure 3 shows TEM photographs of nanofabricated GaAs (100) specimen by the FIB. The change in the morphology of bend contours is similar to that in the Si (100) specimen. On the contrary to the Si (100) case, the defect clusters of a low density were seen in the beam affected area. This could be due to the difference in the mobility of defects generated by Ga ions. The SAD patterns were taken from three different regions in the fabricated area; unaffected matrix (c), beam affected matrix (d) and large particles (e). No diffraction spot in figure 3-d) and -e) demonstrates the microstructural change from single crystal to amorphous. The presence of another amorphous or liquid state, or liquid Ga precipitates, can be deduced from an additional broad hollow ring in figure 3-e).

Figure 4 shows FIB patterned SiO_2 (101) sample. An array of 49 points was patterned in 4 by 4 μm area. In the low magnification image in Fig. 4-a), the points show good arrangement in 7 rows. The bend contour keeps its continuity although a little deformation is observed. In the magnified image in Fig. 4-b), one of the points is shown as a white circle. The size of this circle is about 200 nm, which is in agreement with the beam size. This part of the sample looks to contain dark dots of Ga precipitates in the order of several 10 nm just as in the case of Si, but more detailed observation was prevented because of the tendency toward amorphization of the sample by strong electron beam (Tanaka et al., 1997).

The present study demonstrates one potentiality of the FIB/TEM for the investigation of the compositional and structural changes of semiconductors due to the FIB microlithography. Furthermore, one should point out another potentiality of FIB/TEM in the field of TEM specimen preparations.

EBI-CVD NANOFABRICATION WITH SEM AND TEM

1. Two types of Gas introduction systems and experimentals

First type of gas introduction system for EBI-CVD is attached to a port of the UHV-FE-TEM, which column is evacuated by 7 sputter ion pumps to 5×10^{-8} Pa (Tanaka et al., 1998). The system consists of an external variable leak valve, a gas nozzle which is about 1 mm in diameter, and a heating device. A schematic drawing of the TEM column and the apparatus is illustrated in figure 5. The end of the nozzle is located at the position about

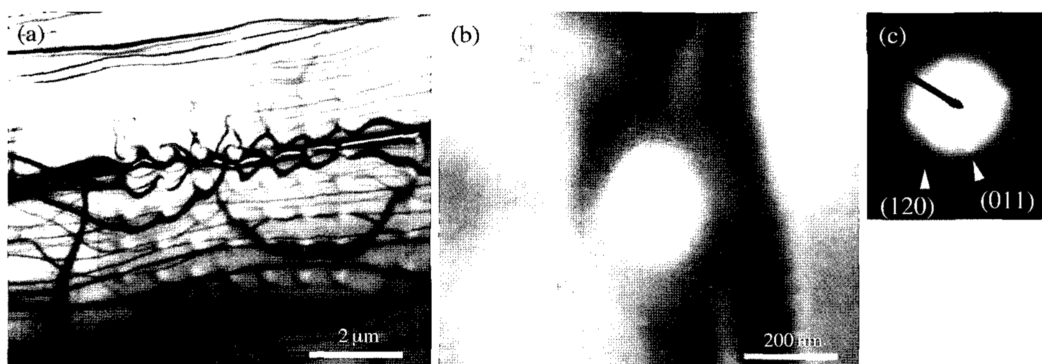

Fig. 4. TEM bright field images of 49 points on a SiO_2 (101) sample. (a) Sub-micron rows are clearly seen, (b) enlarged image of one of the points shows dark dots and slight amorphization and (c) its diffraction pattern.

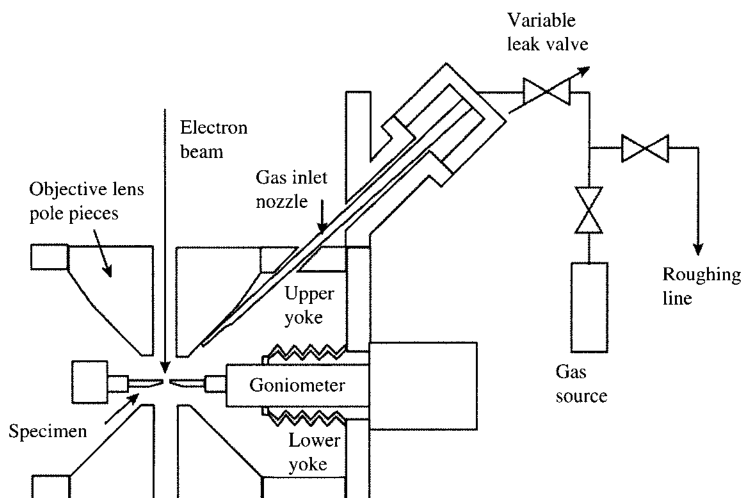

Fig. 5. Schematic illustration of the ultra-high vacuum field emission scanning transmission electron microscope (UHV-FE-STEM) and the externally attached gas inlet system.

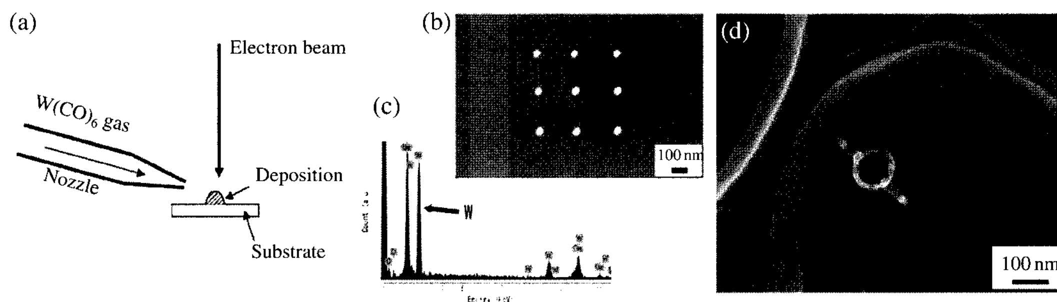

Fig. 6. Schematic illustration of electron beam induced chemical vapor deposition. FE-SEM image (a) and a result of EDS analysis (b) of an array of dots deposited on a Ge substrate using a FE-SEM at 20 kV. (c) SEM image of a self-standing ring grown from edges of a carbon grid into space using a FE-SEM.

3 and 5 mm off the vertical and horizontal from the sample center, respectively. The leak valve is connected to several gas sources. This system makes it simple and easy to change precursors for each experiment. Various precursors, solids, liquids and gases can be attached to the system.

Second type consists of an internal reservoir of the source of gas, mostly a powder, and a gas nozzle of about 0.1 mm in diameter. This apparatus can be mounted on the FE-STEM and the FE-SEM specimen holders and inserted into the microscope column together with specimens. Figure 6-a) illustrates the schematics of this method (Shimojo et al., 2004). The flow rate of gas cannot be controlled externally during the experiments, but pre-set by changing the nozzle diameter.

The substrates were carbon grids, and Si and Ge (111), conventionally polished and ion-milled. The precursor gas was $W(CO)_6$ and the EBI-CVD was done at room temperature. The microscopes were conventional FE-SEM and 200 keV FE-STEM, and UHV-FE-STEM. The electron beam intensity used here was about $5 \times 10^3 \sim 5 \times 10^4$ A/cm^2 and the probe size was about $1 \sim 2$ nm for TEMS and $2 \sim 5$ nm with SEM.

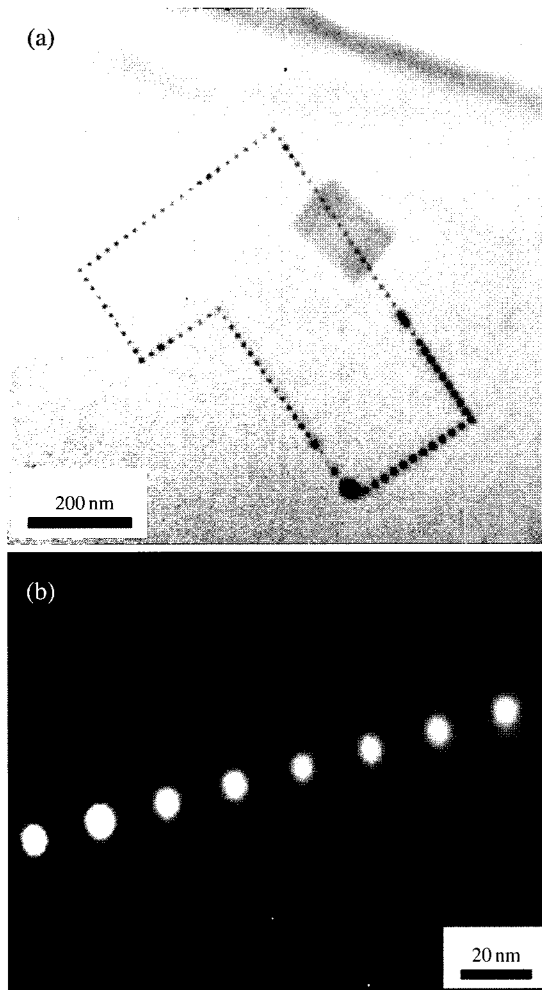

Fig. 7. Bright field (a) and annular dark field (b) images of a dot array deposited using a FE-STEM at 200 kV. The annular dark field image clearly shows the high-Z contrast of W dots.

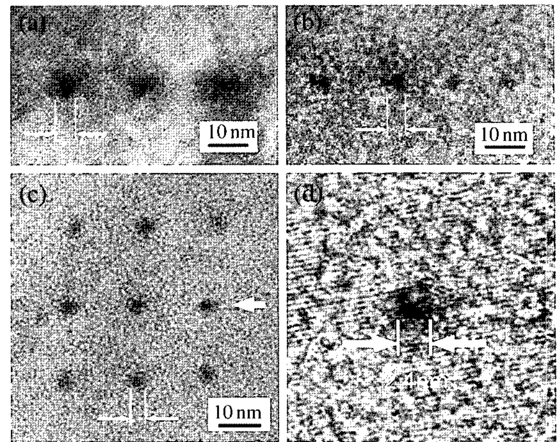

Fig. 8. The partial pressure dependence of the nano-dot size by EBID. (a) Dots formed with 1×10^{-5} Pa, (b) 5×10^{-6} Pa, (c) 2×10^{-6} Pa, and (d) one of the dots in (c) with a size of 2.4 nm.

2. EBI-CVD using FE-SEM, FE-STEM and UHV-FE-STEM for tungsten nanostructures

The bulk substrate of Ge was firstly used for EBI-CVD in the FE-SEM with the chemical analysis of the deposits by EDS. An array of dots deposited with 20 keV electron beam is shown in figure 6-b). Each dot was formed during an electron beam irradiation for 5 s. The diameter of each dot was approximately 15 nm. This size is comparable to the minimum size of such deposits previously reported (Matsui & Ichihashi, 1988) and is smaller than those produced by conventional SEMs (Folch et al., 1995; Koops et al., 1996; Utke et al., 2000). Figure 6-c) shows a result of EDS analysis from a dot. The peaks of W and C are seen in the figure, as well as the peak from the Ge substrate. This indicates that the dots mainly consist of W and small amounts of C, which is consistent with the results by Kislov (Kislov et al., 1996) that tungsten carbide and tungsten oxide were found in addition to pure tungsten in rods produced by EBI-CVD. Figure 6-d) shows a self-standing tungsten ring, about 100 nm in diameter, formed inside a hole of a carbon grid. The deposition started on a certain edge of the grid, and the beam position was subsequently moved into the space to form a ring pattern drawn with a single stroke. The speed of this patterning is about 5.0 nm/s. The minimum line width of the structure grown in a space was about 20 nm. It is definitely possible to fabricate nano-sized three dimensional structures by EBI-CVD.

Si (110) thin films were used as a substrate for deposition with the FE-STEM. The experiments were carried out under the accelerating voltage of the microscope of 200 kV at room temperature. The size of the probe is about 0.8 nm with the current of 0.5 nA. Figure 7-a) shows a bright field image of a dot array formed on a Si substrate. The dots were arranged at a constant interval

by moving the beam position. Most dots were formed at a deposition time of about 0.3 s. Some dots were deposited for 0.5 s and then became slightly larger. A high-angle annular dark field STEM (HAADF-STEM) image is shown in figure 7-b). HAADF-STEM produces Z-contrast images so that the bright dots consist of W, because a W atom is heavier than a Si atom. The minimum size of the W dots is turned out to be about 3.5 nm in diameter. Based on the fact that the size of the fabricated structures is smaller in the FE-STEM than in the FE-SEM at the same gas flux and temperature, the reduction in probe size and the increase in the accelerating voltage are considered to be very effective to fabricate smaller sized nanostructures with EBI-CVD. It was previously reported that the diameter of vertically grown rods would reach about 20 nm due to the secondary electron generation by Monte Carlo simulation (Silvis-Cividjian et al., 2002). However, the present results indicate that the fabrication of nanostructure less than several nm is possible when experimental conditions were properly achieved.

The effect of partial pressure (namely, the flow rate) of precursor gas was precisely examined with UHV-FE-STEM. Figure 8 shows typical TEM photographs of lines and an array of the nano-dots by changing pressure

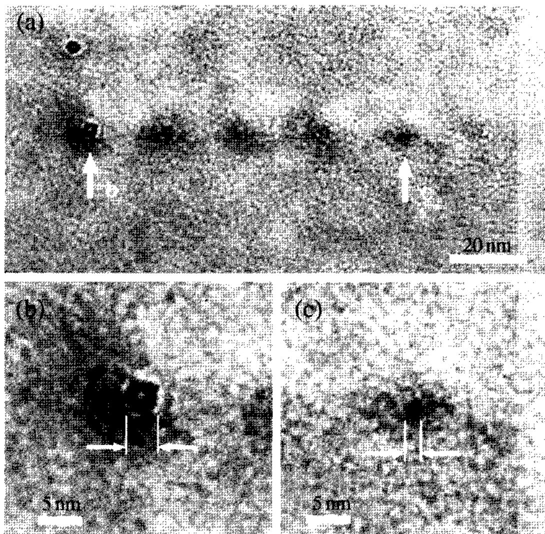

Fig. 9. The irradiation time dependence of the nano-dot size. (a) A line of the dots with different time for 10, 9, 8, 7, 6, and 5 s from left to right. Enlarged images of (b) 10 s (about 4 nm) and (c) 6 s (about 2 nm).

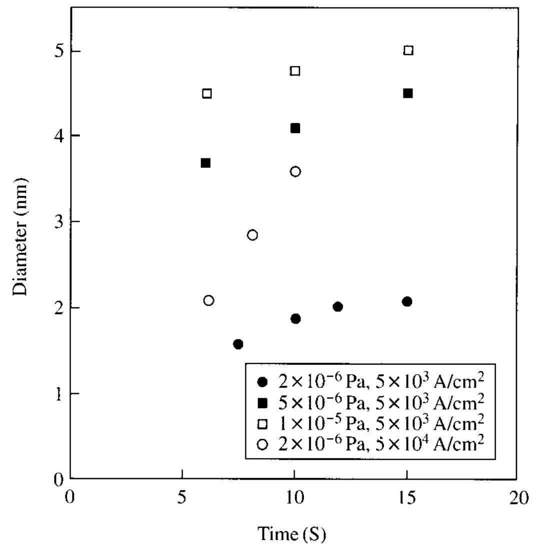

Fig. 10. The relation between the dot-size and the irradiation time as a function of the partial pressure.

of the precursor using a 2 nm-sized probe. The size of the dots becomes smaller as the partial pressures decrease from about 1×10^{-5} Pa, 5×10^{-6} Pa to 2×10^{-6} Pa under the deposition time of about 10 s. In figure 8-a), the average dot size is about 5 nm, while they are about 4 nm and 3 nm in figures 8-b) and 8-c), respectively. The enlarged image of the dots in figure 8-d) shows those lattice fringes of the Si substrate from which the size of the dot is calibrated to be about 2.4 nm. Interestingly, we could seldom observe a dot-formation with the partial pressure of less than 1×10^{-6} Pa, regardless of the beam intensity. We infer that there is a critical partial pressure for the dot fabrication although there is a possibility that the nano-dots were too small to distinguish.

Figure 9-a) shows a line of the nano-dots formed with a constant gas pressure of 2×10^{-6} Pa with changing the deposition time from 10 to 5 s. It is recognized that the size of the dots decreases as the deposition time becomes shorter. The enlarged dots (pointed by arrows) in figure 9-b) and 9-c) were fabricated by 10 and 6 s irradiation, and show the sizes of about 4 and 2 nm, respectively. Similarly to the pressure effect, there is also a critical deposition time for the dot fabrication at a certain gas pressure, because the dot of 5 s deposition is almost impossible to distinguish at 2×10^{-6} Pa.

The dependence of the dot-size upon partial pressure and deposition time is summarized in figure 10. The tendency is obvious: the better vacuum, or the shorter time, the smaller dot. For the current density of 5×10^3 A/cm^2, the partial pressure dependence is more apparent. For the gas pressure of 2×10^{-6} Pa, the current density dependence is also shown. The smallest dot size is about 1.5 nm with 5 s deposition, 1.5×10^{-6} Pa, with probe size of 1 nm. To our knowledge, this is the smallest record ever made by EBI-CVD. Our previous results with a regular FE-STEM show that the 0.275 s irradiation is the shortest for the dot-fabrication and that the dot size is about 3.5 nm at the precursor gas of 10^{-5} Pa. (Mitsuishi et al., 2003). These results suggest that rather partial pressure of the precursor gas most influences the size limit of the dots.

It is known that the electron-beam induced deposits successively follow the process of nucleation, fast growth, and saturation (Silvis-Cividjian et al., 2002). The dots in the saturation regions are what we usually observe after the EBI-CVD in the SEMs with a typical size of 15 nm. The first nucleation stage is influenced by many parameters such as the ambient gas component (background vacuum), the partial pressure of the precursor gas, the surface diffusion of the precursor molecules, the cleanliness of the substrates, and so on. In our system, since the vacuum is kept at such a low level under the strong irradiation of focused electron beam, there are only a few molecules in the area and the nucleation and growth occur rather slowly. The actual reaction rate is given by the convolution of the surface concentration of precursors, the reaction cross section of the adsorbed molecules and the flux of the electrons passing through the adsorbed molecules (Allen et al., 1988). During the dissociation process of the precursor, an indefinite amount of energy is transferred to the molecule from electrons. It is proposed that the energy in excess to that required for bond disruption is stored in vibration degrees of freedom (Koops et al., 1995). Such kind of energy could contribute to the successive or derivative dissociation of the precursors, and hence to the further growth of the deposits. This could be another reason that the better pressure produces smaller nano-dots.

SUMMARY

Nanofabrication with focused ion beam (FIB) and with electron beam induced chemical vapor deposition (EBI-CVD) was reviewed, and position and size controlled fabrication of nano-metals and -semiconductors are demonstrated. Following conclusions were drawn from the results.

(1) A 25 keV FIB system attached to a 200 keV TEM was developed by modifying a specimen chamber to be compatible with the injection of ion beams. The minimum ion beam diameter of about 200 nm and the ion current of 80 pA at the specimen position during the TEM observation were obtained with the working distance of about 100 mm for 25 keV Ga ions.

(2) The process of the FIB lithography of Si (100), GaAs (100) and SiO_2 (101) is found to depend on the combination of the physical sputtering and ion implantation. Ga ions sputtered out substrate atoms uniformly, but were partially implanted on the surface and at the shallow portion beneath the surface and precipitated as nanoparticles.

(3) When decomposable gases with electron beams, such as $W(CO)_6$, were introduced at the beam irradiated areas, nano-metal dots can be formed by EBI-CVD depending upon the beam diameter. The diameter of the dots was reduced to about 3.5 nm with the FE-STEM, while those were limited to about 15 nm in diameter with the FE-SEM. Self-standing structures were successfully fabricated.

(4) Using UHV-FE-TEM, the size of the dots can be controlled by changing the time for irradiation and the partial pressure of the precursor. Due to both the small probe of 200 keV-TEM and the controlled partial pressure of the gas, the dot size of less than 2 nm is achieved. The results suggest the possibility of further improvement of the resolution by combining the small probe (STEM) and the controlled gas supply (UHV).

REFERENCES

Allen TE, Kunz RR, Mayer TM: J Vac Sci Technol B6 : 2057, 1988.

Aristov VV, Yu Kasumov A, Kislov NA, Kononenko OV, Matveev VN, Tulin VA, Khodos II, Gorbatov YA, Nikolaichik VI: Nanotechnology 6 : 35, 1995.

Assayag GB, Vieu C, Gierak J, Sudraud P, Corbin A: J Vac Sci Technol B11 : 2420, 1993.

Folch A, Tejada J, Peters CH, Wrighton MS: Appl Phys Lett

66 : 2080, 1995.

Furuya K, Ishikawa N: Rad Effects Defects Solids 124 : 61, 1992.

Furuya K, SaitoT: J Appl Phys 80 : 1922, 1996a.

Furuya K, Saito T: J Electron Microsc 45 : 291, 1996b.

Kislov NA, Khodos II, Ivanov ED, Barthel J: Scanning 18 : 114, 1996.

Kohlmann-von Platen KT, Chiebek J, Weiss M, Reimer K, Oertel H, Brunger WH: J Vac Sci Technol B11 : 2219, 1993.

Koops HWP, Kaya A, Weber M: J Vac Sci Technol B13 : 2400, 1995.

Koops HWP, Schossler C, Kaya A, Weber M: J Vac Sci Technol B14 : 41055, 1996.

Matsui S, Ichihashi T: Appl Phys Lett 53 : 842, 1988.

Mitsuishi K, Shimojo M, Han M, Furuya K: Appl Phys Lett 83 : 2064, 2003.

Shimojo M, Mitsuishi K, Tameike A, Furuya K: J Vac Sci Technol B22 : 742, 2004.

Silvis-Cividjian N, Hagen CW, Kruit P, v.d. Stam MAJ, Groen HB: Appl Phys Lett 82 : 3514, 2003.

Silvis-Cividjian N, Hagen CW, Leunissen LHA, Kruit P: Microelectronic Eng 61-62 : 693, 2002.

Tanaka M, Furuya K, Saito T: Appl Phys Lett 68 : 961, 1996.

Tanaka M, Furuya K, Saito T: J Surf Anal 3 : 435, 1997.

Tanaka M, Furuya K, Saito T: Mat Res Soc Symp Proc 438 : 313, 1997a.

Tanaka M, Furuya K, Saito T: Nuc Inst and Met B127/128 : 98, 1997b.

Tanaka M, Furuya K, Takeguchi M, Honda T: Thin Solid Films 319 : 110, 1998.

Tanaka M, Shimojo M, Han M, Mitsuishi K, Furuya K: Surf Int Anal 37 : 261, 2005.

Tanaka M, Shimojo M, Mitsuishi K, Furuya K: Appl Phys A78 : 543, 2004.

Utke I, Hoffmann P, Dwir B, Leifer K, Kapon E, Doppelt P: J Vac Sci Technol B18 : 3168, 2000.

White CW, Wilson SR, Appleton BR, Young FW Jr.: J Appl Phys 51 : 738, 1980.